Coordination at solid surfaces: investigations on the atomic scale by field ion microscopic techniques

Jochen H. Block

Fritz-Haber-Institut der Max-Planck-Gesellschaft, Faradayweg 4-6, D-1000 Berlin 33

Abstract - Three experimental methods enable us to study solid surfaces on the atomic scale:
1. Electron Microscopy can achieve atomic resolution in both transmission and reflection modes under special conditions, producing promising results. However, surface studies are hampered by bad vacuum conditions in most instruments.
2. Scanning Tunneling Microscopy has caused wide spread interest due to the experimental simplicity. Not only have a great number of structural problems been solved, tunneling spectroscopy also reveals electronic surface properties.
3. Field ion microscopic techniques display atomic surface structures, allow experiments with single atoms and can identify the chemical nature of single atoms or molecules and their binding energies. Pulse techniques are used for kinetic measurements and determination of intermediates in heterogeneous catalysis. Cluster-ions with low internal energy can be field desorbed. The disadvantage of this method is that samples have to drawn into tips and high electrostatic fields have to be applied.
Examples are given to show how field ion microscopy can determine surface structure, bond direction and surface reconstruction, and how the surface motion of individual particles can be measured and used to derive fundamental thermodynamic data.
With field pulse desorption both surface structure sensitive reactions $(Ni + CO \rightarrow Ni(CO)_4)$ and insensitive reactions (decomposition of methanol) are observed. Photon-stimulated field desorption is applied to study properties of cluster ions.

INTRODUCTION

One of the recent scopes in coordination chemistry was defined as being concerned with the interaction of organic and inorganic ligands with metallic or semiconducting elements. Such interactions are of particular importance at solid surfaces. If a metal atom is not an isolated one but part of an extended solid surface its reactivity with ligands may be completely different. The chemical bond which can be formed between this metal atom and ligands depends on the number and position of its neighbours in the solid. Surface phenomena like chemisorption or surface reactivity are therefore frequently "structure sensitive", i.e. because of their symmetry the surface planes (111), (100), etc., interact differerently with ligands, surface edge atoms and different kinds of steps also display differing properties.

One further complication arises from the fact that surfaces of solids reconstruct. For energetic reasons, atoms at and near the surface choose new lattice positions which differ from the periodicity of the bulk. Therefore surface atoms take on unusual coordination, radical-like chemical bonds form which are sensitive to adsorbed molecules, they in turn may alter surface radical bonds and surface structure. The complexity of these phenomena are the reasons for the unpredictibility of surface properties and the statement by the Swiss physicist Wolfgang Pauli (1900-1958): "Solid surfaces are invented by the devil".

A large number of modern surface science techniques have been developed since 1958 in order to learn about the behaviour of surfaces in chemistry, to understand phenomena like heterogeneous catalysis, corrosion and properties of interfaces in nanometer electronic devices.

In most of these techniques samples with extended surface areas, for instance single crystals planes of ≈ 1 cm^2 surface area have been studied and integral properties of 10^{14} to 10^{15} surface atoms were then measured. Even if the analyzed area is reduced to ≈ 1 µm^2, which is possible with different modern micro-analytical techniques, there are still some 10^7 surface atoms probed simultaneously. For a series of surface reactions which are expected to be surface site specific and possess particular "active centres", the analysis of individual surface sites is desired. In the present contribution, analytical methods for surface studies on the atomic scale will be described and, in particular, field ion microscopic methods will be applied to explore surface properties and reactivity in real space and real time.

EXPERIMENTAL METHODS

Atomic resolution in imaging solid surfaces can be achieved by three different analytical methods:
1. Electron Microscopy (ref. 1) (Ernst Ruska, 1932)
2. Field Ion Microscopy (ref. 2) (Erwin W. Müller, 1951) and
3. Scanning Tunneling Microscopy (ref. 3) (G. Binnig and H. Rohrer 1982)

1) The many years of development in electron-microscopy have recently brought interesting applications to surface properties. A few examples may be mentioned. In transmission electron microscopy - which usually cannot discriminate between surface and bulk atoms - the structure of Au-surface layers could be imaged by directing the electron beam to the edge of an Au(100) (1x1) surface (ref. 4). Evidence for surface Shockley partial dislocations is found. The result is correlated with the known (5x20) reconstruction to a hexagonal overlayer since the dislocations possess a pseudo-hexagonal core structure. This implies a dislocation mechanism for the phase transformation from (1x1) to (5x20). It is proposed that pipe diffusion along the dislocation cores or mass transport via dislocation glide or climb (lines) could explain the rapid atomic migration required during the phase transition from the (1x1) to hexagonal structures.

Mono-atomic steps have recently been analyzed by reflection electron microscopy (ref. 5) and used to investigate structural changes during catalytic surface reactions, like the CO-oxidation on Pt(100)- and Pt(111)-single crystal planes. Using an intensity enhanced Bragg reflection for imaging the surfaces, a surface roughening on the atomic scale could be observed. The Pt(100) plane was much more strongly attacked than the Pt(111)-surface. A similar crystallographic preference will be discussed later for CO on Ni-planes in the field ion microscopic experiments.

The application of electron microscopic techniques to problems of surface science are frequently hampered by the bad vacuum of most instruments. A further point of consideration must concern the destructive property of the electron beam. Interesting developments are presently being pursued and further experiments under controlled gas pressures and with improved imaging procedures will, certainly, contribute further to the understanding of solid surfaces.

2) In the few years since 1982, Scanning Tunneling Microscopy (STM) has found wide-spread applications. The early convincing experiment was the imaging of the reconstructed (7x7) structure of Si(111) in real space /6/, which corresponded with the model of Takayanagi. The STM-technique has also been applied to the investigation of surface reactions with a local resolution of individual atoms. The Al(111)-surface displays an unexpected, high contrast with a corrugation of 0.3 Å. (ref. 7). Carbon impurity atoms are adsorbed in three-fold coordination sites and change the local electron distribution in such a way, that the tunneling current vanishes in the immediate vincinity of the C-atoms. The chemisorption of oxygen shows two subsequent steps: initially small O_{ad}-islands are formed statistically without structure-sensitivity. The nucleation of surface oxide is then preferentially seen at steps (ref. 7).

The development of STM has proceeded rapidly. For a rigorous description, the structure determination of the probing tip very important. In addition to structure information, electronic properties of surfaces can be probed by tunneling spectroscopy. Non-conducting surfaces may be analyzed by the atomic-force microscope (ref. 8). The well established structure information from STM has already been applied to many problems in surface coordination chemistry. For analytical purposes, however, a direct chemical identification of surface compounds is not possible with STM.
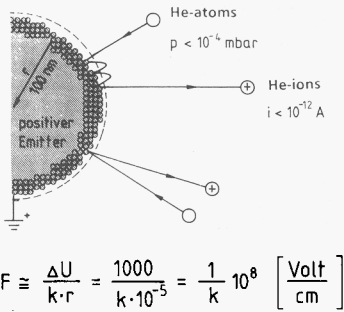
3) In this comparison field ionization techniques are favourable. The mechanism of field ionization, the field ion imaging procedures, and appropriate analytical methods will be described in detail.

THE FIELD ION MICROSCOPE (FIM)

When a solid surface is imaged on a screen with a few cm diameter and magnification of 10^6, then the imaged object has to have dimensions on the 10^{-6} cm scale. In FIM the imaged object is a half-spherical tip with a radius between 10^{-6} and 10^{-4} cm (100...10 000 Å). The field-ion-microscope which images individual atoms (Fig. 1) is a simple projection microscope without any ion-optical device. The magnification is simply determined by the radius, r, of the half-spherical tip and the distance R to the image plane (luminescent screen or image amplifier). With a typical tip radius of r = 10^{-5} cm (1000 Å) and a distance, R, of 10 cm the magification is R/r ≈ 10^6.

The structural information of the tip surface is transfered to the luminescent screen by ions of an inert imaging gas. Ions, like He^+, Ne^+, etc. with a certain mass have to be used, since due to Heisenbergs' uncertainty relation, electrons cannot reach atomic resolution (only ≈20 Å). Ions are formed from the impinging image gas atoms by the field ionization process. With the potential ΔU of several kV between the positive tip and the luminescent screen (or a counter electrode) a field strength F ≈ 10^8 V/m is obtained near the surface of the field emitter tip. In this field, image gas atoms are field ionized by tunneling of an electron from the gas atom into the emitter surface. The positive ion, which is created during the tunneling process, experiences the positive tip potential and is accellerated towards the luminescent screen. Since the electric field vectors are approximately normal to the tip surface, a constant magnification of this surface is nearly obtained.

Principles of FIM

He-atoms
$p < 10^{-4}$ mbar

He-ions
$i < 10^{-12}$ A

100 nm

positiver
Emitter

The Microscope

R

$$F \cong \frac{\Delta U}{k \cdot r} = \frac{1000}{k \cdot 10^{-5}} = \frac{1}{k} \, 10^8 \left[\frac{\text{Volt}}{\text{cm}} \right]$$
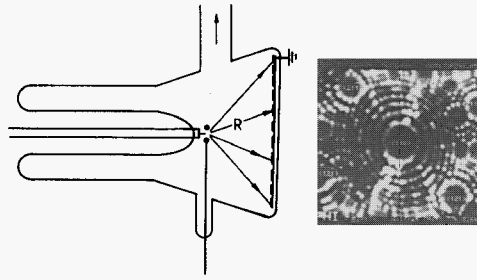
Fig. 1. Principles of FIM. Upper Part: The tip emitter (magnified) is the half-spherical end of a needle, radius 10 to 1000 nm. With a positive potential, ΔU, of a few kV a field strength, F, of 10 to 60 V/nm is reached. Impinging image gas atoms, He, are field ionized by tunneling of electrons. Positive ions are accelerated towards the screen (lower part) or an image amplifier. The tip surface is imaged with a magnification of 10^6.

The quantitative description of the field ionization process in front of the ion emitter surface is still not possible and a complete theoretical description of field ion images still remains a task for theoreticians. The following qualitative description can account for the contrast in field ion images. The local brightness of the field ion image is caused by the local current intensity of ionized particles. The ionization probability at the emitter surface depends on the local field strength and therefore on the charge distribution at the surface, the field penetration into the bulk and the tunneling probability, due to the overlap of electron wave functions of the surface and the imaging gas atom. Field ion images display very characteristic patterns, not only because of their crystallographic structures, but also due to different electronic properties of the tip materials.

FIELD DESORPTION AND FIELD EVAPORATION

The field strengths in front of the field emitter can be increased such that adsorbed molecules (surface ligand structures) will be field desorbed as ions. At even higher field strengths, the top atomic layer of the emitter material can field evaporate in ionic form. Individual ionic species are then analyzed chemically in the atom-probe (ref. 8), which is an extension of the field ion microscope incorporating a time-of-flight or magnetic sector mass spectrometer (Fig. 2). Field desorption of adsorbed layers and field evaporation of the top layers of the bulk field emitter

Emitter
Image Intensifier
Detector
2 m Flight Length
Start
Stop
HV Pulse
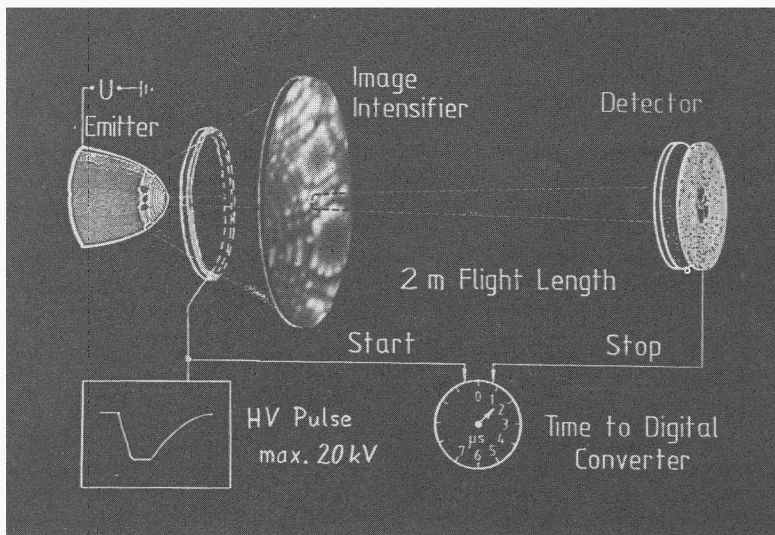max. 20 kV
Time to Digital Converter

Fig. 2. The Atom-Probe: The field ion microscope (left with magnified tip) acts as a field desorption microscope. Surface atoms or molecules are field desorbed as positive ions when a negative HV-pulse is applied to the counter-electrons. A few ions desorbing from a selected area of the tip pass through the probe hole and reach the detector. The flight time (and mass-to-charge ratio) is evaluated by measuring the time between the start of the field pulse and the stop, arrival of the individual ions.
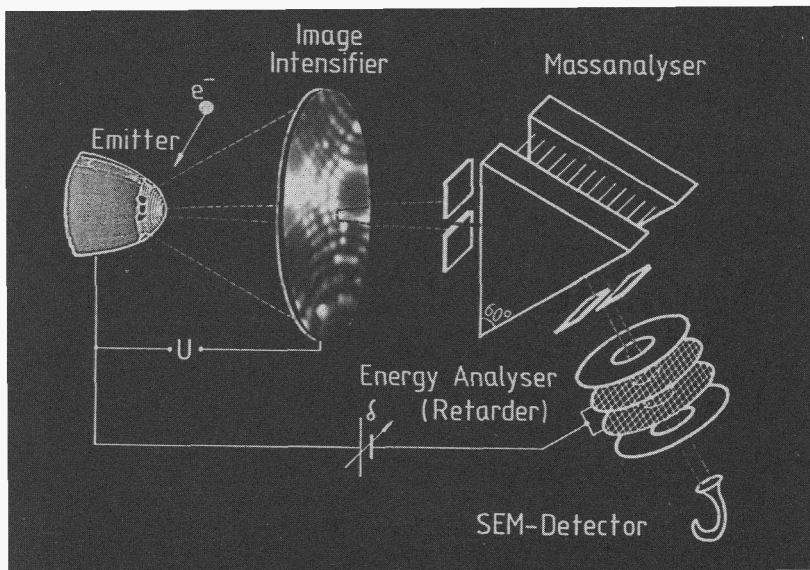
Fig. 3.   Atom Probe with Magnetic Sector Analyzer. An energy analyzer (retarder grid) is
connected to the emitter potential via a battery potential δ. By changing β an integral energy
analysis of field desorbed ions is obtained. Due to the great voltage drop in front of the emitter
(few Volt/Å) and a precision for β of better ±0.1 V, the origin of ions in front of the surface can be
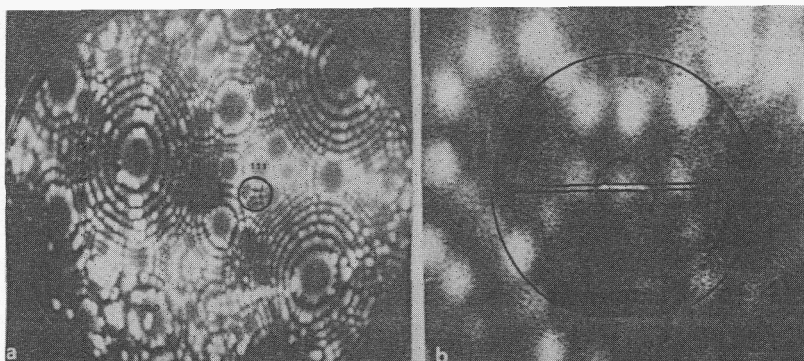determined to better than 0.1 Å.

Fig. 4.   Local Resolution for Probing Electronic Surface Properties with the Magnetic Sector
Atom Probe (according to N. Ernst). (a) He-FIM of W(111)-oriented probe hole (black ring below
(111)); (b) probe hole with the projection of the mass spectrometer entrance slit, tungsten atom
marked white, slit in the inner ring.

material represent extremely sensitive surface (Fig. 3) analytical tools. An individual surface
atom or adsorbed molecule is first characterized according to its crystallographic position by
imaging in the FIM mode.

In the field ion image the position of the individual atom or molecule can first be located at a
certain crystallographic position, (Fig. 4), a terrace, a step-site etc. The probe hole then is located
at this position and the particle is field desorbed by a short field-, photon- or electron-pulse. The
chemical identification follows from the measured mass-to-charge ratio in the time-of-flight mass
spectrometer. This represents the most sensitive surface analytical measurement, and allows
individual surface particles whose crystallographic position has been determined to be identified.

It has to be mentioned that the described technique may face difficulties for different reasons:
inability to imaging certain species, field induced instabilities of surface compounds, etc.
Furthermore, conclusions on surface processes can be derived only from the statistics of a certain
number of events, not from single individual observations as described so far.

The advantage of FIM methods in imaging and analyzing individual surface atoms is combined
with the requirement to prepare the samples as tips shape. This art of preparation has been
extended to many metals, semiconductors and even high temperature superconductors, as
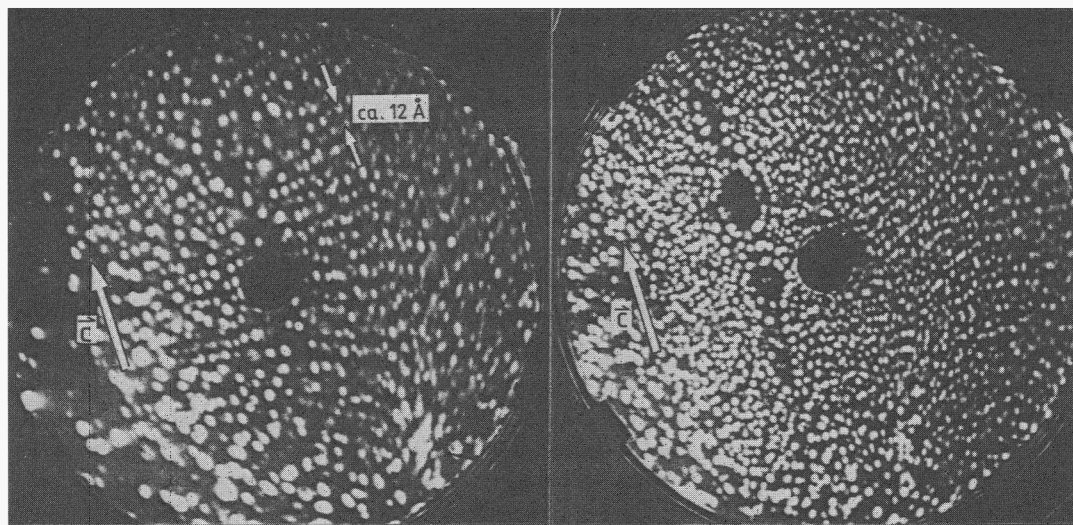described in (ref. 9) and demonstrated in Fig. 5.

Fig. 5. Field Ion Image of a High Temperature Superconductor. Sample: Y Ba_2 Cu_3 O_{7-x} imaged with Ar at 78 K. The layer structure 12 Å lattice distance, perpendicular to the c-axis. Left: slow field evaporation in Ar (11.25 kV); Right: field evaporation in Ar(12.6 kV).

A further restriction in FIM techniques is given by the extremely high electrostatic field which has to be applied and which may change surface properties dramatically. Systematic experimental and theoretical studies of "high field surface chemistry" have been started (ref. 10) and it has been shown that the field strength can be considered as an extensive reaction parameter which is of importance in different areas of surface chemistry (promotors in heterogeneous catalysis etc.).

SURFACE STRUCTURE AND SURFACE DIFFUSION

The atomic resolution of FIM has been used to directly image surface reconstruction in real space and to compare these images with diffraction patterns (LEED). From these patterns it is well known that the Ni (110)-surface reconstructs after adsorption of hydrogen and models like "paired row" and "missing row" have been discussed. A field ion image study by G. Kellogg (ref. 11) clearly shows that the missing row model applied. In Fig. 6 several rows of nickel atoms in a Ni(110)-surface are imaged using Ne-imaging gas. A temperature treatment to 200 K in Ne
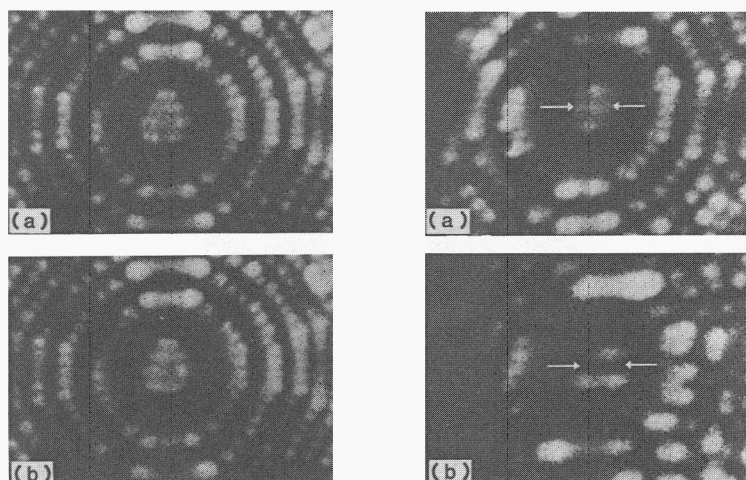

Fig. 6. Direct observations of the deuterium-induced surface reconstruction of the Ni(110) plane (according to G.L. Kellogg).
Left hand side: Field ion micrographs of a Ni(110) plane recorded (a) before and (b) after heating the sample to 200 K in pure Ne. No changes in the surface structure are observed.
Right hand side: Field ion micrographs of Ni(110) plane recorded before and after heating the sample to 175 K with 1×10^{-8} Torr deuterium present. The three chains of Ni atoms comprising the topmost (110) layer reconstructed to two chains with a missing row. The small arrows point to the row of atoms in (a) which is "missing" in (b).

leaves the structure unchanged (a+b left-hand side). A similar treatment in D_2 at 175 K reconstructs the surface in such a way that one row of Ni-atoms is missing. The missing row model (lower left) describes the process. Surface diffusion of individual surface atoms or of clusters of surface atoms has been investigated by several research groups. A wealth of data on surface interactions is obtained for self-diffusion as well as hetero-diffusion. A few examples may illustrate the potential of this technique. Quantitative observations of single atom motion on metal surfaces are made by depositing individual atoms by an evaporation process onto a selected surface. The surface is imaged at low temperature ($T \approx 20$ K), then heated without field for a certain time ($\approx 10s$) to a diffusion temperature ($T = 100$ K, etc). The tip is then recooled to the imaging temperature to determine the new positions of the adatoms. From the statistical evaluation of atomic positions, partition functions and finally binding energies and pre-exponential factors for surface diffusion can be obtained.

As an example the determination of binding energies of Rh on a W(211)-surface by Wang and Ehrlich (ref. 12) is shown in Fig. 7. Within the trough of a W(211) plane (see model at the top of Fig. 7) 20 lattice positions exist in this row. They are not imaged per se since at this flat part of the surface the field strength is insufficient. The rhodium atoms are, however, clearly revealed in the micrographs. At a diffusion temperature of 197 K their positions are centred around 18 central sites in an asymmetric manner. The frequency of occupation of different sites is shown below in Fig. 7. Sites near the edges have properties which differ from those in the centre of the plane and edges directed along (100)-differ from those along (111)-planes on account of next nearest neighbour effects. The determination of the mean square displacements of the atoms, yields the diffusivity and from the temperature dependence binding energies can be evaluated.

Surface diffusion of Rh on W(211) has been described for this simple case in terms of a hard-sphere model. In other cases an exchange between adatom and substrate-atom has been measured or a concerted diffusion of different atoms simultaneously has been observed. Diffusion processes have to be thought of in terms of making and breaking chemical bonds and the change in bond-order during atomic movement determines the energetics of the diffusion process.
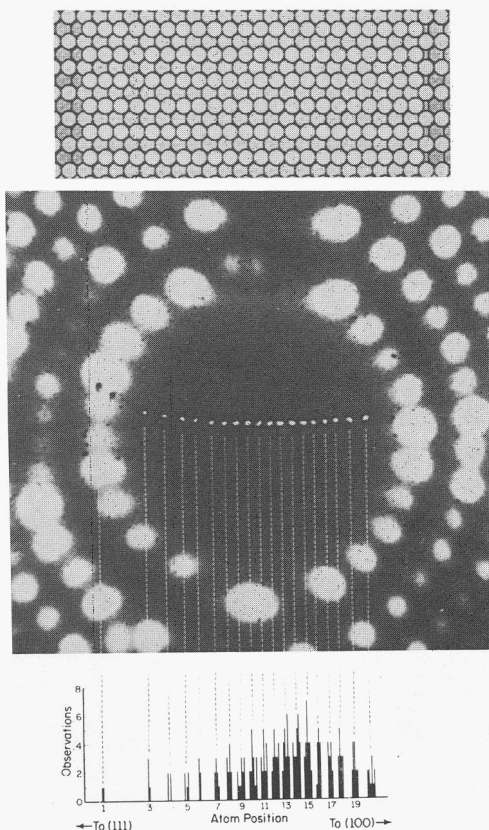

Fig. 7.   Determination of binding sites for rhodium atom. Superimposed upon the field ion micrograph of a W(211) plane in the centre are the locations of a rhodium atom observed after diffusion at 197 K. The observations are clustered around 18 central sites. A plot of the frequency of these observations on an enlarged distance scale is shown below, together with a hard-sphere model of the (211) plane above (according to S.C. Wang and G. Ehrlich).
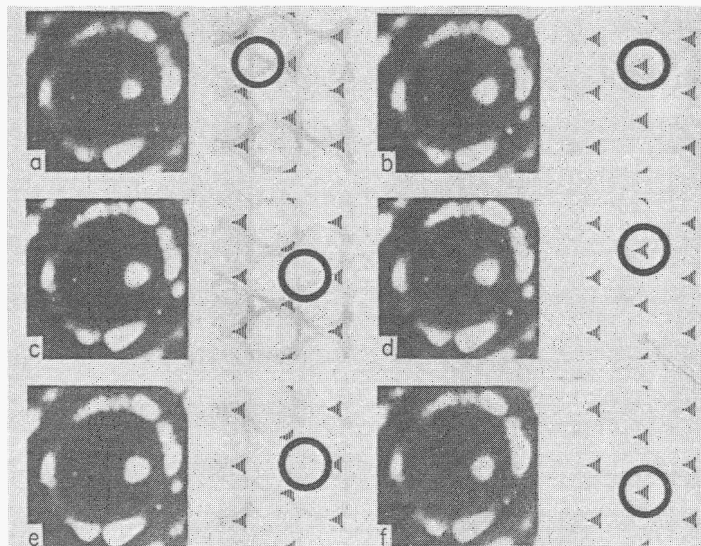
Fig. 8. Imaging and diffusion of individual iridium adatoms on Ir(111). Field ion images of single iridium atoms are triangular, indicative for direction of chemical bond. Iridium adatom on Ir(111), observed after diffusion at 93 K. The adatom location is illustrated on accompanying schematic to the right of field ion image. Number of 10 s intervals between displacements: (b) 33, (c) 3, (d) 29, (e) 6, (f) 42 (according to S.C. Wang and G. Ehrlich).

Recently Wang and Ehrlich /13/ observed unusual asymmetric image spots when imaging Ir-adatoms on a Ir(111)-surface. As shown in Fig. 8, field ion images of single iridium adatoms atoms are triangular. This asymmetry is an indication of chemical bond directions. The apex of the triangles of Ir-atoms can either point in the [211]-direction or in the opposite one. We have to remember that the (111)-plane of a face-centred cubic crystal displays two kinds of adsorption sites: bulk sites with the local geometry of an a fcc-lattice, and surface sites with the local environment of a hcp-lattice. During these experiments it could be shown that bulk sites show the apex of triangular spots pointing to the left and for surface sites the apex points to the right. Ir - adatoms prefer to adsorb on surface sites, but may also occupy bulk sites. Both sites are involved in diffusion processes. The triangles are caused by the local distribution of charge density, which influences the local field distribution and tunneling probability of the image gas atoms.

SURFACE REACTIONS

Selected crystallographic areas of the field emitter surface can be choosen to investigate surface - plane or site specific reactions. For this purpose, FIM studies are combined with pulsed field desorption mass spectrometry (PFDMS) (ref.s 14, 15): a surface reaction proceeds at the tip surface while the gas supply (10^{-3}-10^{-8} Torr) is kept constant. After a certain reaction time ($t_R = 10^{-6}$ ...10^{1} sec) a field pulse completely removes the adsorbed layer. Instantaneously reactants, intermediates and products of the surface reaction are desorbed and analyzed in the mass spectrometer. After the pulsed field desorption step, which lasts some hundred nanoseconds, a new reaction step with the same t_R starts. Up to 10^3 or 10^4 reaction steps are repeated. Then a different t_R-value is choosen. For intensity reasons usually some 100 surface sites of the emitter area are monitored simultaneously. At short t_R the initial increase in surface coverage (sticking coefficients) is measured. With increasing t_R-values, relaxation-times for intermediates or products are observed, and at long reaction times, t_R, thermal adsorption and desorption processes may govern the surface coverage and steady state surface coverages can be measured. Thus, PFDMS allows to determine the kinetic parameters of a surface reaction (ref. 16) to be determined.

THE REACTION OF CO WITH NI-SURFACE A FIM STUDIES

Figure 9 (a) shows an ion micrograph of a clean nickel crystal, field evaporated in neon at 80 K. The middle part shows the relatively extended system of (111)-layers. The step height of one layer is equal to the lattice step height. Slightly to the right in the lower part are the layers of the (100)-plane. The transient areas between the central (111) and the peripherical (111) and (100) planes are subdivided neatly up to very high index planes.
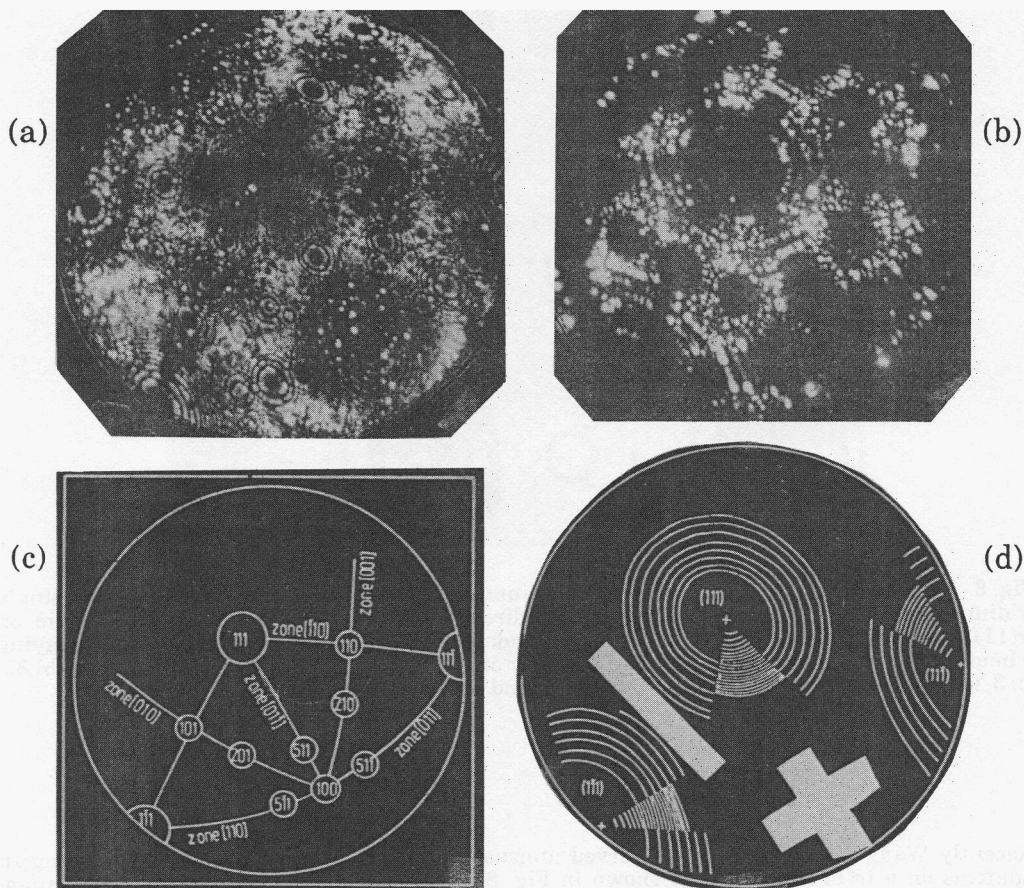
Fig. 9. (a) (upper left) FIM of clean Ni before reaction (Ne 80K); (b) (upper right) FIM of Ni after reaction with CO; (c) (lower left) *Müller* indices of the Ni-emitter; (d) (lower right) illustration of main structural changes.

The surface structure of Fig. 9 (b) was obtained after the crystal was reacted under fieldfree conditions with CO at 1.3 mbar pressure and 373 K. By comparison to the initial state of the nickel crystal, there were conspicious alterations of the crystal shape after reaction with CO:

1. Areas of {111} planes were increased.
2. At half angles between the central {111} and the peripherical {110} planes there were planes flanked by {210} and with {511} respectively. The small top layer of planes showed a cross with a quandratic form in <110> orientation.
3. The number of rings around the poles was reduced compared with the initial state.

These alterations of crystal habitus can be explained by applying arguments from the theory of crystal growth. As discussed in detail in (ref. 17), these changes in morphology are due to the high reaction rate of Ni-kink atoms of (111) planes along <001> rows. Thus, the formation of surface carbonyl compounds on nickel is a site-specific chemical reaction. The intermediate products of this reaction are nickel-subcarbonyls.

INVESTIGATION OF THE REACTION Ni + CO BY PFDMS

The mechanism of the intermediate carbonyl formation was studied by PFDMS (ref. 18). In Fig. 10, the time dependence of the intermediates $Ni(CO)$, $Ni(CO)_2$ and $Ni(CO)_3$ are shown. A rather long delay time is observed for formation of the dicarbonyl. From these results the conclusion can be drawn that at least two CO-molecules have to be attached to a Ni-kink site atom in order to remove it from the anchored lattice position. Kink-site positions of the fcc-lattice have nearly the same binding energies for (100)- and (111)-planes. The reason that (111)-planes are prefered in the carbonyl reaction may be due to the fact that three nearest neighbours are missing in the (111)-plane, whereas for the (100)-plane there are only two. The mobile $Ni(CO)_2$-surface species preferentially formed on Ni(111) then reacts to $Ni(CO)_3$ and finally to $Ni(CO)_4$, which is volatile and therefore cannot be detected by this surface analytical method. Detailed aspects of this site-specific reaction are discussed in the literature (ref.s 18 and 19).
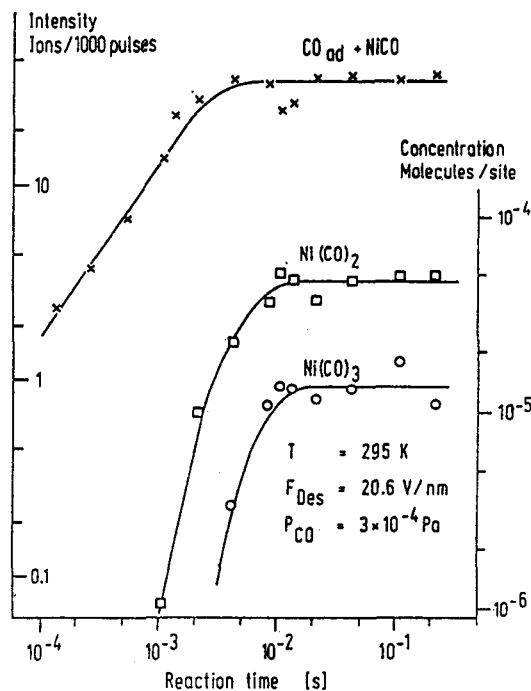
Fig. 10. Variation of surface concentration of nickel carbonyls with reaction time t_R. Monitored area: 9.5 nm², containing 150 surface sites. Impingement rate: 450 CO molecules/s.
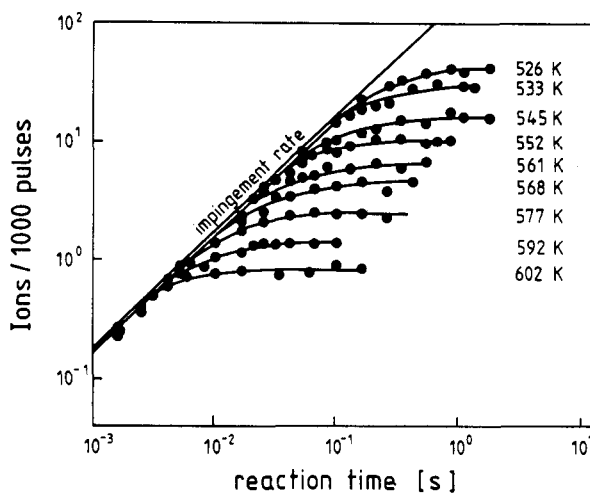
Fig. 11. Temperature dependence of the mean lifetime, τ, of NO on Pt; the values refer to mearurements on a stepped surface region with (111)-orientation of the terraces.

THE REACTION OF NO WITH Pt- AND Ru-SURFACES

NO-chemisorption on Pt is surface-plane specific, showing non-dissociative molecular adsorption in the Pt(111)-region and dissociative adsorption for the Pt(100)-stepped surface (ref. 20).

Applying field pulse techniques in the region of the stepped Pt(111)-surface one can measure the kinetics of adsorption and the thermal equilibration of the adlayer by varying the reaction time ($100 \ \mu s < t_R < 10$ s) as described above.

The measurement of the mean lifetime, τ, at different temperatures yields the activation energy, E_d, for thermal desorption and the pre-exponential term, τ_o, of Frenkels' equation, $\tau = \tau_o \cdot \exp (E_d/kT)$. Measurements performed for mean lifetimes at different temperatures for NO adsorption on about a hundred atomic sites in the monitored area are presented in Fig. 11. Since only NO^+-ions were desorbed, the ion intensities are directly correlated to surface concentrations of NO_{ad}. The kinetic parameters for the thermal desorption process are found to be $E_d = 139$ kJ/mol and $\tau_o = 3 \cdot 10^{-14}$ s. Recently, molecular beam reflection spectroscopy studies (MBRS) on the adsorption and thermal desorption of NO from Pt(111) have yielded the same values (ref. 21). There is agreement that the binding energy E_d is correlated with a high binding energy molecular adsorption state, which is formed at < 20 % maximum surface coverage. This surface state displays interesting field-induced dissociation as described below.

On the stepped Pt(001)-surface molecular and dissociative adsorption are found (Fig. 12). The molecular adsorption occurs with a coverage-independent value c˘ the sticking coefficient (0.6.....0.86). The mean lifetime, τ, of NO at 543 K is $\tau \approx 2 \times 10^{-1}$ s. At lonκr reaction times, $t_R > 10^{-1}$ s, PtO^+-ions are observed. PtO is indicative for dissiociated NO. Chemisorbed oxygen is field desorbed in the form of PtO^+, nitrogen desorbs thermally and is therefore not detected by PFDMS. From the results of Fig. 12 it has to be concluded that NO-dissociation occurs only after the Pt(001) surface is covered with NO (ads).

Ru(001)-surfaces are still more reactive to NO-dissociation. At $T \approx 500$ K NO-molecules oxidize Ru as demonstrated in Fig. 13. Reaction time variations are compared for Pt(001) and Ru(001). The Ru (001) forms surface oxide immediately ($T < 10^{-3}$ sec) after impact of NO. The data for Pt (from Fig. 11) are given for comparison.
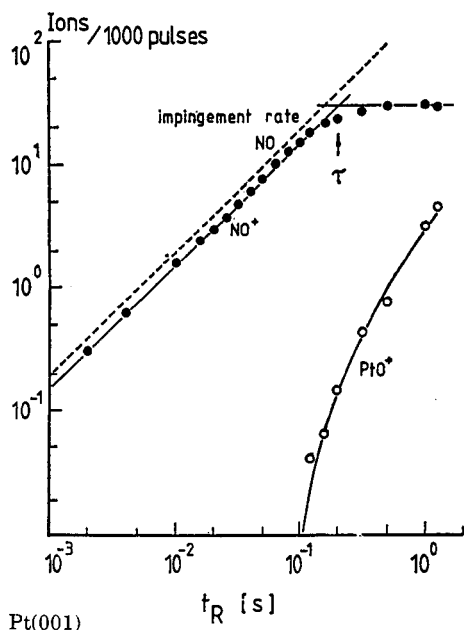
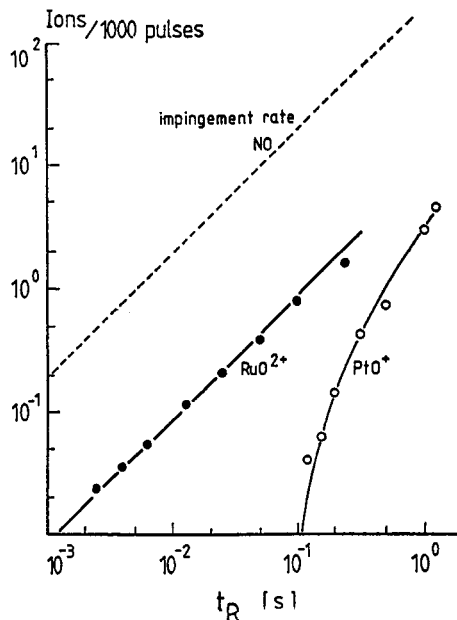Pt(001) t_R [s]

Fig. 12   Fig. 13

Fig. 12. Dependence of NO^+ and PtO^+ intensities on reaction time, t_R. NO pressure: 1.3×10^{-5} Pa; T=543 K, F_D=28 V/nm, τ=mean lifetime of molecular adsorbed NO; impingement rate: 0.19 molecules/s into the monitored area. The NO-adsorption Pt(001) shows that dissociation of NO occurs only after the adlayer is saturated with molecular NO. Chemisorbed oxygen is field desorbed as PtO^+.

Fig. 13. NO-chemisorption on Pt(001) and Ru(001); NO intensities are not shown. On Ru(001) only dissociative chemisorption of NO is observed. NO-pressure:1.3×10^{-5} Pa; impingement rate: 0.19 molecules/s into the monitored area; tip temperatures: 503 K for Ru, 543 K for Pt; pulsed field strength: 30 V/nm for Ru, 28 V/nm for Pt. The ion intensities refer to the same size of the monitored area.

FIELD-INDUCED FRAGMENTATION OF NO ON Pt (111)

Electrostatic fields of the order of 10 V/nm may constrain surface reactions into new pathways. These influences are apparent from dissociation, fragmentation, association and charge transfer. For NO a field-induced dissociation is found on Pt(111)-surfaces (ref. 22). For evaluating these field influences, the steady reaction field, F_R, was successively altered, without changing other reaction parameters.

In the lower steady field range only NO^+ ions are detected (Fig.14). At moderate fields, various other species, N_2O^+, N_2^+ and O^+, appear in addition. The intensities of these species increase steeply with rising F_R values. The onsets for N_2O^+ and O^+ desorption are coincident at F_R 4 V/nm, the N_2^+ ions appear somewhat later. The intensities of N_2O^+ are observed to reach about
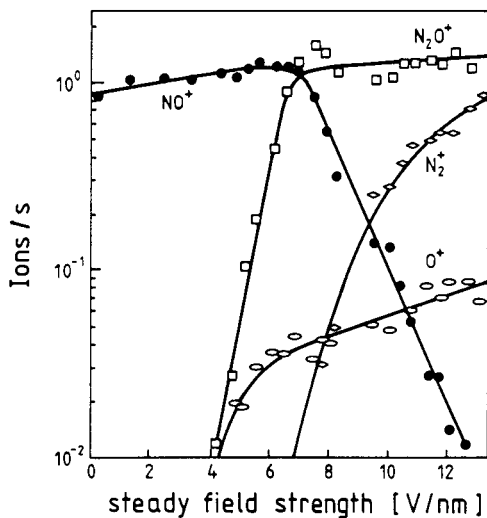

Fig. 14. Field induced decomposition on Pt, measured at a stepped surface with (111) orientation of the terrace. The steady field strength, F_R, is varied and the pulse field is adjusted so that the desorption field is constant at $F_D = 24$ V/nm; NO pressure: 6.7×10^{-5} Pa, T = 296 K.

the same level as those of NO^+ for small F_R. Further augmentation of the field strength is associated with decreasing NO^+ rates. Both N_2^+ and O^+ intensities increase continuously within the measured range of F_R values, however, the O^+ ions are much less abundant.

The general result of Fig. 14 is the field induced decomposition of NO on Pt(111) into N_2O, N_2 and O_{ads}; a theoretical account can be given for this decomposition reaction by applying the ASED-MO-method (atom superposition and electron delocalization molecular orbital-calculation) (ref. 23). It can be shown that the electrostatic field forces the NO-molecule to tilt and an overlap of oxygen orbitals with surface wave functions weakens the N-O-bond.

THE CATALYTIC DECOMPOSITION OF METHANOL

a. Field microscopy with rhodium-emitters

Using the technique of FIM, the surface structure of Rh before and after long time reaction with methanol, was imaged. The method successfully applied to the Ni/CO system (ref. 24) is suited to detect changes in the substrate topography. Figure 15 a shows a field ion micrograph of a Rh tip, cleaned by field evaporation and imaged in neon at 78 K. The accompanying map (Fig. 15 b) gives the location of dominant low- and high-index planes seen in the images. As is characteristic of a field-evaporated end form high- and low-index planes have rather small diameters. The {001} plane is located in the centre of the micrograph and four {111} planes are seen at the periphery. The discrete bright spots in the image present atoms of the net plane boundaries.
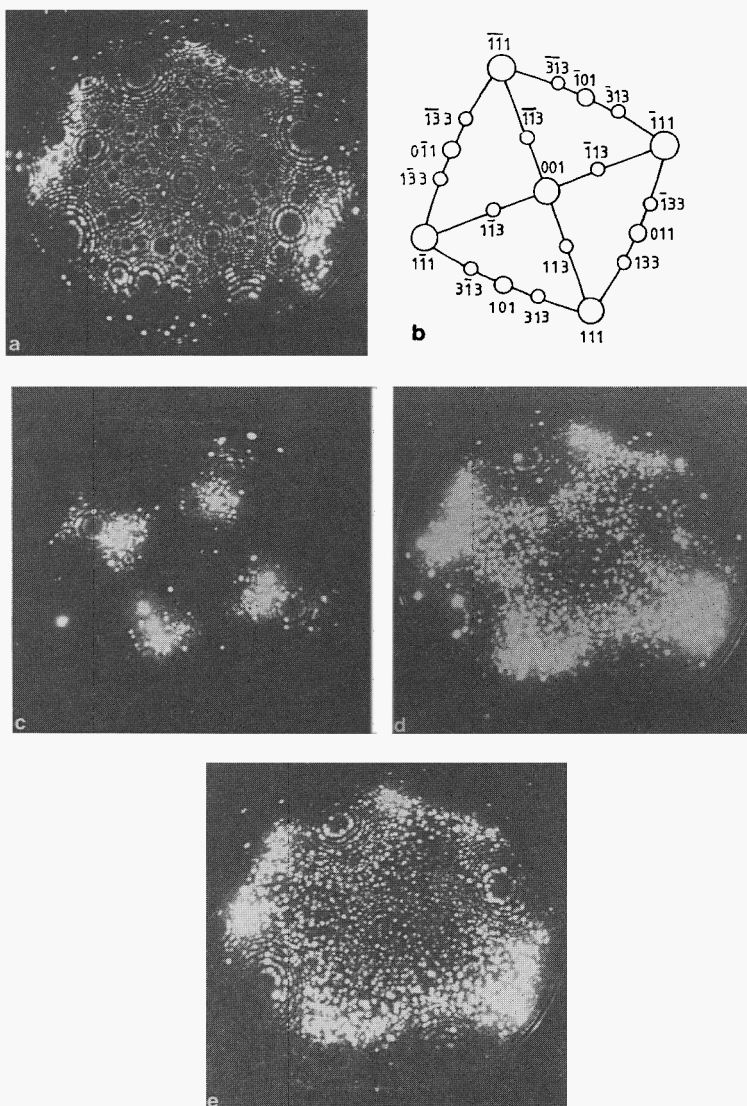

Fig. 15. FIM images in neon of Rh tip taken at 78 K before and after exposure to CH_3OH at p = 2 Pa and at 295 K for 10 min; (a) clean surface, imaging field at 35 V/nm: (b) map of dominant planes. Field ion images after successive increase of field strength c, d, e.

The clean Rh tip was exposed to 2 Pa CH$_3$OH for 10 min at various temperatures such as 295, 323, 373, and 423 K. Exposure times of 10 min were sufficient in these experiments since at prolonged times the same results were produced. The FIM images obtained thereafter represent forms attained after adsorption and reaction at the chosen temperature. The ion images were taken at rather low field strengths so that no field evaporation of the substrate occurred. If there were drastic changes in the sizes of the planes and/or the heights between the net planes after the reaction, they could be unambiguously attributed to dissolution of the reactant. Figures 15 c-e show a selection of neon FIM images taken at 78 K after reaction with CH$_3$OH at 295 K. As the imaging field was adjusted stepwise from small to higher values, surface are as became gradually visible, thus exposing more and more of the surface structure. At moderate fields (Fig. 15 c), the {011} planes are seen in addition to the adsorbate molecules which produce extremely bright image spots. At 32.4 V/nm (Fig. 15d), the central (001) and the {111} appear, whereas the (011) are hidden by more bright image spots. Comparison of the diameter of these planes before and after the methanol decomposition reaction shows that there are no detectable changes. Also no other dominant higher-index facets were developed. The very slightly reduced top layer of the central (001) plane observed after reaction (Fig. 15 d) must be disregarded since such very small changes were also sometimes detected after annealing the Rh crystal without methanol present. Treatments at higher temperatures lead to the same observations, i.e., no topographical changes can be deduced by FIM following methanol adsorption and decomposition on the Rh surface in the temperature range of 295-423 K.

No structural changes could be detected which would indicate a preferential surface plane in the catalytic CH$_3$OH-decomposition. However, field ion images (Fig. 15 c-15e) show a rather spotty structure. This structure may be due to displaced Rh-atoms or to remainding chemisorption layers of CO, CH$_3$CO, etc. It may be that atoms of the top-layers of Rh are displaced during the CH$_3$OH-decomposition. In contrast to the Ni/CO case no net topographical changes can be seen. The decomposition of CH$_3$OH on Rh-under these experimental conditions - has to be considered as non-structure-sensitive.

b. Measurements by PFDMS

Mass spectrometric analysis of field desorbed ions from Rh(001)-and Rh(111)-oriented emitters showed no differences, in accordance with FIM results. At temperatures below T = 450 K the mass spectra yield, in addition to the hydrogen species H$^+$, H$_2^+$, H$_3^+$ mainly CO$^+$, CH$_3^+$, H$_2$O$^+$. Only if a steady reaction field, F$_R$ ≈ 4 V/nm is applied, CH$_x$O-species (x = 1,2,4) detected. With increasing temperature mass spectra show decreasing intensities of CH$_2$O$^+$ at T > 320 K, CH$_3^+$ at T > 420 and Rh(CO)$_x^+$ at T > 500 K. These findings can be explained by the following mechanism. At room temperature CH$_3$OH decomposes to strongly chemisorbed products (CO, CH$_3$ etc.) which prevent further reaction of CH$_3$OH. If reaction fields are applied CH$_x$CO-intermediate structures are stabilized. The catalytic reaction can only occur, when these strongly adsorbed intermediates desorb and liberate reaction sites. This site-blocking and inhibition of the catalytic methanol decomposition has been observed with other surface analytical methods. Above the desorption temperature of CO, which is T > 500 K for Rh and T > 450 for Ru, the rate determining step of the catalytic CH$_3$-OH decomposition is the stepwise fission of C-H bonds, as shown by PFDMS-measurements.

FIELD DESORPTION OF CLUSTER IONS

One other aspect which is of interest for coordination chemistry concerns the particular preference to form cluster-ions by field desorption. During field desorption, ions of low internal energy may be produced. With photon- or electron-stimulated field desorption, additional energy may be added. From appearance potential measurements, the structure of neutral clusters which are ionized by electron tunneling can often be determined.

A few examples will briefly be reported: H$_3^+$-ions are field desorbed from a neutral H$_3$-species, which has a linear structure (H-H-H), an ionization potential of 10.4 eV, an adsorption energy (on a tungsten kink site atom) of 1.8 ± 0.1 eV and, at 78 K, a lifetime between 10 µs and 300 µs (ref. 29). According to theoretical calculations the ground state of a linear H-H-H structure is a few tenth of an electron volt less stable than the separated particles H$_2$, H. Theoretical work by H. J. Kreuzer demonstrated, however, that the H$_3$-structure is field stabilized. Experimentally, the field ion energy-spectroscopy (appearance spectroscopy) of H$_3^+$ was measured and compared with Ar$^+$. By this method the origin of field desorbed ions with respect to the distance from the image plane is determined with a precision of better than 0.1Å. From experimental data, a linear H-H-H structure has been deduced. The lifetime (10 µs < τ < 300 µs) was determined with the aid of photon-stimulated field desorption (ref. 30). H$_3$-and H$_3^+$-clusters are of particular interest because their properties could be evaluated from first principle calculations.

Another interesting question in coordination chemistry concerns the stability of multiply charged cluster-ions. The question is whether charge repulsion forces can be balanced by attractive chemical binding forces. Experimental work with photon-stimulated field evaporation concerned the stability of doubly charged triatomic metal clusters (ref.s 31 and 32). Field evaporation, induced by short laser pulses, is used as a source for producing cluster ions. Besides

atomic ions, which are field evaporating from most of the metals at low temperatures, a temperature pulse, caused by photon-impact, induces atomic agglomeration and cluster formation. The investigation of triatomic clusters of metals like Cu, Ag, Au, Ni, W, etc., revealed that some of the doubly charged species are detectable while others are absent. A comparison with other experimental data leads to a simple empirical rule; a stability criterion is derived by balancing the attractive bond energies of neutral clusters and the repulsive Coulomb energies within the doubly charged ions. These results give an interesting explanation for the phenomenon of "Coulomb-Explosion" in multiply charged ionic species.

FIELD DESORPTION OF WATER CLUSTERS

During field desorption cluster ions with low internal energy can be formed. This technique therefore is suited to study properties of ionic species with low internal binding energies.

Synchrotron radiation was used to study the photon-induced field desorption from a water covered field emitter (ref.s 33 and 34). Above a threshold photon energy of 7.1 eV, the desorption of a variety of water clusters, $(H_2O)_n \cdot H^+$, $n = 1,....., 15$, is observed. The cluster distribution (Fig.16) shows only traces of H_3O^+- and $(H_2O)_2 \cdot H^+$-ions. With a maximum at $(H_2O)_3 \cdot H^+$ the intensities decrease towards $(H_2O)_{15} \cdot H^+$, the largest detectable species. The missing intensities of H_3O^+ and $(H_2O)_2 \cdot H^+$ can be explained by energetic reasons. The threshold energy, which corresponds with the optical absorption maximum of liquid water, is found to be independent of cluster size and substrate material. The abundance of clusters decrease roughly exponentially with increasing cluster size and depends also on substrate temperature and photon energy. The analysis of the cluster distribution reveals an energy increment of 9 meV per water molecule which seems to be correlated to the frustrated translational energy of water molecules on metals. Basic RRK-theory arguments can be applied to explain the cluster distribution.
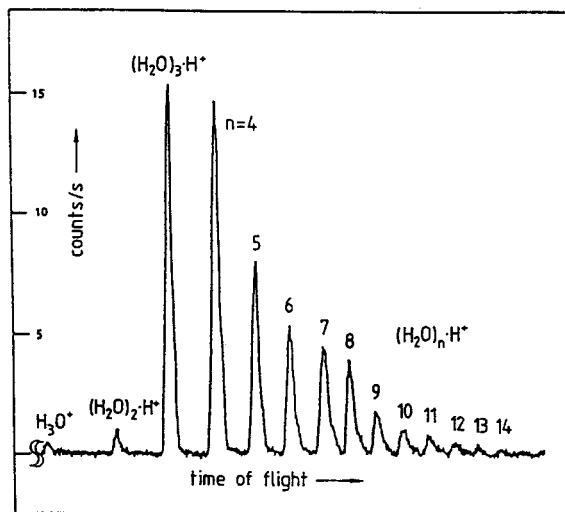

Fig. 16. Time-of-flight mass spectrum of water clusters field-desorbed with photon pulses from a synchrotron-source (HASYLAB), photon energy: 24.8 eV, emitter: silver tip, tip temperature: 54 K, water pressure 2×10^{-8} mbar, tip potential ΔU: 10 kV.

CONCLUSIONS

Field ion microscopy and- mass spectroscopy have been proven as valuable methods in exploring properties of solid surfaces on the atomic scale. Only few systems have been investigated so far however they demonstrate that a great variety of phenomena govern this interesting chemistry of solid surfaces.

Acknowledgement

REFERENCES

1. E. Ruska *"The Early Development of Electron Lenses and Electron Microscopy "*, Hirzel Verlag Stuttgart, 1980.
2. E.W. Müller and T.T. Tsong *"Field Ion Microscopy - Principles and Applications"*, Elsevier, N.Y., 1969.
3. G. Binnig, H. Rohrer et. al., Appl. Phys. Lett., 40, 178 (1982).
4. L.D. Marks and D.J. Smith, Surf. Sci., 157, L367(1985).
5. Y. Uchida, G. Lehmpfuhl and R. Imbihl, Surf. Sci., in press.
6. G. Binnig, H. Rohrer, Ch. Gerber and E. Weibel, Phys. Rev. Lett., 50, 120 (1983).
7. J. Wintterlin, H. Brune, H. Höfer and R.J. Behm, Appl. Phys., A47, 99 (1988).
8. E. W. Müller, J. A. Panitz and S. B. McLane, Rev. Sci. Instr., 39, 83 (1968).
9. N. Ernst, G. Bozdech and A. J. Melmed, Journ. de Physique, C6- 49, 45 (1988).
10. J. H. Block, H. J. Kreuzer and L. C. Wang , Surf. Sci., accepted July 1990.
11. G. L. Kellogg, Phys. Rev., B 37, 4288 (1988).
12. S. C. Wang and G. Ehrlich, Surf. Sci., 206, 451 (1988).
13. S. C. Wang and G. Ehrlich, Surf. Sci., 224, L997 (1989).
14. J. H. Block, in "Methods and Phenomena" Vol. 1, ed. A. W. Czanderna, Elsevier 1975, 379.
15. J. H. Block, Mitt. Chem. Ges. d. DDR, 36, 121 (1989).
16. J. H. Block and N. Kruse, React. Kinet. Catal. Lett., 35, 11 (1987).
17. W. A. Schmidt, J. H. Block and K. A. Becker, Surf. Sci., 122, 409 (1982).
18. D. B. Liang, G. Abend and J. H. Block, Surf. Sci., 126, 392 (1983).
19. N. Kruse, G. Abend and J. H. Block, J. Chem. Phys., 91, 577 (1989).
20. J. H. Block and N. Kruse, Anales De Quimica de la Real Societad, Española de Quimica 84, 292 (1988).
21. C. T. Campbell, G. Ertl and J. Segner, Surf. Sci., 115, 309 (1982).
22. G. K. Chuah, N. Kruse, J. H. Block and G. Abend, Journ. de Physique, C6-48, 493 (1987).
23. H. J. Kreuzer and L. C. Wang, Surf. Sci., in press.
24. G.-K. Chuah, N. Kruse, W.A. Schmidt, J.H. Block and G. Abend, J. Catal,. 119, 342 (1989).
25. G.-K. Chuah, N. Kruse, J.H. Block and G. Abend, Journ. de Physique, C6-49, 215 (1988).
26. N. Kruse, G.-K. Chuah, G. Abend, D.L. Cocke and J.H. Block, Surf. Sci., 189/190, 832 (1987).
27. G.-K. Chuah, N. Kruse, G. Abend and J.H. Block, Journ. de Physique, C7-47, 435(1986).
28. J.H. Block, *Chemistry and Physics of Solid Surfaces*, Vol. IV, Springer Ser. Chem. Phys. 20, 407 (1982), ed. R. Vanselow and R. Howe, Springer New York.
29. N. Ernst and J.H. Block, Phys. Rev., B29, 7092 (1984).
30. W. Drachsel, S. Nishigaki, N. Ernst and J.H. Block, Int. J. Mass Spectrom. Ion Phys., 46, 297 (1983).
31. Th. Jentsch, W. Drachsel, and J.H. Block, Chem. Phys. Lett., 93, 144 (1982).
32. W. Drachsel, Th. Jentsch, K.A. Gingerich and J.H. Block, Surf. Sci., 156, 173 (1985).
33. S. Jaenicke, A. Ciszewski, J. Dösselmann, W. Drachsel, J.H. Block and D. Menzel, Journ. de Physique, C6-49, 191 (1988).
34. J. Dirks, W. Drachsel and J.H. Block, Journ. de Physique, C8-50, 153(1989).